NDT&E International 129 (2022) 102655

Contents lists available at ScienceDirect

NDT and E International

journal homepage: www.elsevier.com/locate/ndteint

Thickness measurement optimisation for permanently installed inductively coupled ultrasonic transducer systems

Yangjie Chen *, Jie Zhang, Anthony J. Croxford, Paul D. Wilcox

Department of Mechanical Engineering, University of Bristol, University Walk, Bristol, BS8 1TR, United Kingdom

ARTICLE INFO

Keywords:
Calibration
Inductive coupling
Permanently installed sensor
Structural health monitoring
Ultrasound

ABSTRACT

An inductively coupled ultrasonic transducer system (ICTS) is a lightweight, wireless, battery-free, and low-profile (0.5 mm thick) permanently installed sensor system for measuring remaining wall thickness at fixed locations for structural health monitoring. In an ICTS, a slight variation in measured thickness has been observed that is dependent on the misalignment between the handheld probing unit and the permanently attached sensor. A correction algorithm has been developed to improve the ultimate thickness measurement performance of ICTS even with misalignment. The algorithm eliminates a system delay from the measured first arrival time based on the measured bandwidth of the cross-talk signal. Crucially, the algorithm does not require identification of the second back-wall echo as this is not always possible if the back surface of the structure is badly corroded. The correction algorithm has successfully improved the thickness measurement precision from 0.19 mm to 0.07 mm. A higher accuracy of thickness measurement is also achieved, with the mean of the corrected thicknesses equals to the true thickness to ±0.01 mm. The algorithm also enabled the detection of a thickness loss of 0.09 mm. The improvement on thickness measurement performance is important for manual inspection, and future robotic interrogation which will become more viable as up to 20 mm lateral misalignment and 10 mm vertical misalignment can be accommodated.

1. Introduction

In non-destructive evaluation (NDE) and structural health monitoring (SHM), ultrasonic waves are widely used to assess structural integrity [1–5]. Measuring and monitoring remaining wall thickness of structures provides critical information for evaluating the safety of valuable assets such as oil storage tanks and pressure vessels. Measurement is used to confirm that the thickness of the inspected component exceeds the minimum safe thickness, and allows scheduling of repair and replacement of components to reduce downtime [6,7]. Manual UT is a common thickness measurement tool in NDE. However, many factors such as probe coupling, inspector and procedure errors limit its thickness measurement performance. On the other hand, permanently installed sensors effectively eliminate the inspector and procedural errors.

One such permanently installed approach is the inductively coupled ultrasonic transducer system (ICTS) developed by Zhong et al. [8] to measure and monitor remaining wall thickness at fixed locations over time. The ICTS benefits from its lightweight, wireless, battery-free, and low-profile (0.5 mm thick) sensor design. ICTS is currently activated only by manual inspection with a probing unit, but it is also suited for robotic inspection by deploying crawlers or unmanned aerial vehicles (UAVs) to activate sensors and take thickness measurements.

There is a growing interest in robotic non-destructive testing (NDT) and numerous robots have been developed for NDT inspection purposes [9–13]. This drives development of robotic solutions in NDT including taking measurements from permanently attached sensors. Robotic deployments enable easier access to places at elevated height or under hostile conditions. For example, ICTS sensors installed on large vessels require scaffoldings for inspectors to access, increasing the inspection time and costs. Robotic inspection also ensures safety of inspectors. Generally, robotic deployments suffer from positioning error accumulated while navigating on structures [9,14,15]. Progress has been made on improving positioning accuracy using an accelerometer [14]. However, better positional accuracy typically comes at increased cost and complexity.

An ICTS employs three coils to transmit and receive ultrasonic information wirelessly through electromagnetic coupling. The

* Corresponding author.
E-mail addresses: yangjie.chen@bristol.ac.uk (Y. Chen), j.zhang@bristol.ac.uk (J. Zhang), a.j.croxford@bristol.ac.uk (A.J. Croxford), p.wilcox@bristol.ac.uk (P.D. Wilcox).

https://doi.org/10.1016/j.ndteint.2022.102655
Received 16 November 2021; Received in revised form 18 March 2022; Accepted 13 April 2022
Available online 17 April 2022

transmitting and receiving coils in the probing unit are inductively coupled with a secondary coil in the sensor. A piezoelectric transducer is physically connected to the inspected structures surface through adhesive couplant, and is activated by the secondary coil when a thickness measurement is required. Instead of averaging, chirp excitation is employed to maximise the Signal-to-Noise ratio (SNR) so that the signal can be obtained in a single excitation for ease of manual data collection [16]. The received signal is post processed to a conventional ultrasonic A-scan, enabling standard NDE procedures to be applied to calculate the thickness using time of flight.

Practical experience of utilising ICTSs suggests that the measured thickness is dependent on the position of the probing unit relative to the sensor when the measurement is being made (this is explored more fully in later sections of the paper), which is assumed to be caused by the change in mutual inductance between the coils with position. The misalignment of the probing unit relative to the sensor can be parameterised by 6° of freedom (DOFs), specifically, 3 translational DOFs and 3 rotational DOFs. This paper focuses on how misalignment in the translational DOFs affects the received signals. This is because translational misalignment is more common in manual inspection where typically an operator places the probing unit either directly onto the sensor itself or onto the surface of a protective cladding layer over the sensor. This is also expected to be the case in future automated inspections. The translational DOFs are lateral offset in X and Y axes, and vertical standoff in the Z axis. The rotational misalignment is also briefly studied for the completeness of the investigation.

The effect of alignment on thickness measurement precision in an ICTS was experimentally measured to be 0.19 mm (see section 2.4) and is much smaller than manual UT repeatability errors, which can be up to 1 mm [6,17], but it limits the ultimate performance of the system. Therefore, this paper aims to explore methods to improve the measurement performance of an ICTS system to detect ever smaller changes in absolute thickness of structures consistently, without requiring perfect alignment of the system. Successful development of this study will ease manual inspection and enable robotic interrogation at a lower positioning cost.

Thickness is often calculated using either the arrival time of the first ultrasonic echo from the back-wall of a component (termed here “first arrival time”), or by the difference between the arrival times of the first and second back-wall echoes (termed here “peak-to-peak time”). Peak-to-peak time is considered more accurate because the first arrival time contains various system delays (e.g., due to wave propagation time through the adhesive between the piezoelectric transducer and the structure). However, if the back-wall of a structure is badly corroded, the second back-wall echo may be unidentifiable because the transmitted ultrasonic wave is scattered by the rough surface at each reflection. Therefore, thickness estimation based on the first arrival time is preferable as it enables an ICTS to make measurements on components with a higher level of corrosion.

This paper attempts to improve absolute thickness accuracy even with misalignment in the ICTS. To achieve this, experiments were set up to investigate the system behaviour under different misalignment conditions, followed by development of a correction algorithm to improve the absolute thickness accuracy even in the case of poor alignment.

The experimental setup and system response are presented in section 2. The development of the correction algorithm is demonstrated in section 3, followed by demonstration of the measurement performance improvement of the proposed algorithm in section 4. Section 5 describes a quick method of generating the correction curve for the algorithm. The paper ends with a short conclusion in section 6.

2. System behaviour of the inductively coupled ultrasonic transducer system

To investigate how the thickness measurement is affected by the relative position between the probing unit and the sensor in the ICTS, experiments were carried out. This is a key first step to ensure the magnitude of the effect is understood and enable the development of subsequent correction approaches.

2.1. Experiment setup

The ICTS shown in Fig. 1(a) consists of an arbitrary waveform generator and acquisition system (TiePie Handyscope HS5), a printed circuit board (PCB) containing concentric transmitting and receiving coils as the probing unit, and a sensor containing a secondary coil and a piezoelectric transducer (15 mm × 5 mm), which is bonded to the structure under test. The centre frequency of the transducer used here is 5 MHz. The sensor is installed on an aluminium plate which is machined to a uniform thickness of 9.95 mm ± 0.01 mm measured using a micrometre.

The arbitrary waveform generator is connected to the probing unit to transmit an electromagnetic signal to the piezoelectric transducer via inductive coupling between the transmitting and secondary coils, the sensor embedded on the structure is activated by this signal and generates an ultrasonic bulk wave which travels through the structure and is reflected by the back-wall. When a reflected wave reaches the sensor current is generated in the secondary coil, which is then received by the acquisition system through the inductive coupling between the secondary and the receiving coils.

To understand the system behaviour as the relative position between probing unit and sensor changes, the probing unit is secured in a custom plastic holder mounted on a commercial scanning system (SMD 03–00, Ultrasonic Sciences Limited). The scanning system is used to precisely control two important positional parameters, lateral offset and vertical standoff, to determine their effects on the received signals. As shown in Fig. 1(b), the lateral offset is defined as the horizontal distance (i.e., in the X–Y plane) between the centre of the probing unit and that of the sensor. The vertical standoff describes the vertical separation (i.e., on the Z-axis) between the centre of the probing unit and sensor.

2.2. Signal post processing

The system is activated at multiple locations with controlled offset and standoff. Chirp excitation with the same bandwidth as a Gaussian-windowed tone burst with 10 cycles and centre frequency of 4.8 MHz is used. Empirical testing shows that a 4.8 MHz centre frequency provides the optimal compromise between signal amplitude and ring down time. The chirp is generated by altering the phases of the frequency components of the underlying Gaussian-windowed tone burst to extend the temporal duration of the signal by a specified factor (here a factor of 400 is used) [16]. The received signal is dechirped to produce a conventional time domain signal (A-Scan) at each location. Fig. 2(a) shows an example A-scan recorded at 0 mm offset and 10 mm standoff. Each A-scan is analysed both in the time and the frequency domain in post processing.

In the time domain, the signal comprises cross-talk, the first echo, the second echo, and subsequent unshown echoes that fall into the noise level. The cross-talk is caused by the current induced in the receiving coil by the transmitting coil when a signal is being transmitted from the probing unit; its amplitude is very high because the transmitting and receiving coils are concentric. The peak amplitudes and arrival times of the cross-talk, first, and second echoes are extracted from the magnitude of the Hilbert transform of the A-scan. The arrival time difference between the cross-talk and the first echo provides the first arrival time, T. The arrival time difference between the first and the second echo is the peak-to-peak time, ΔT. To minimise temporal quantisation error, the time domain signal is up-sampled from 50 MHz to 500 MHz using Fourier interpolation.

Additional parameters for possible misalignment correction are extracted from the signal in the frequency domain. Post processing in the frequency domain only focuses on the spectrum of the cross-talk region

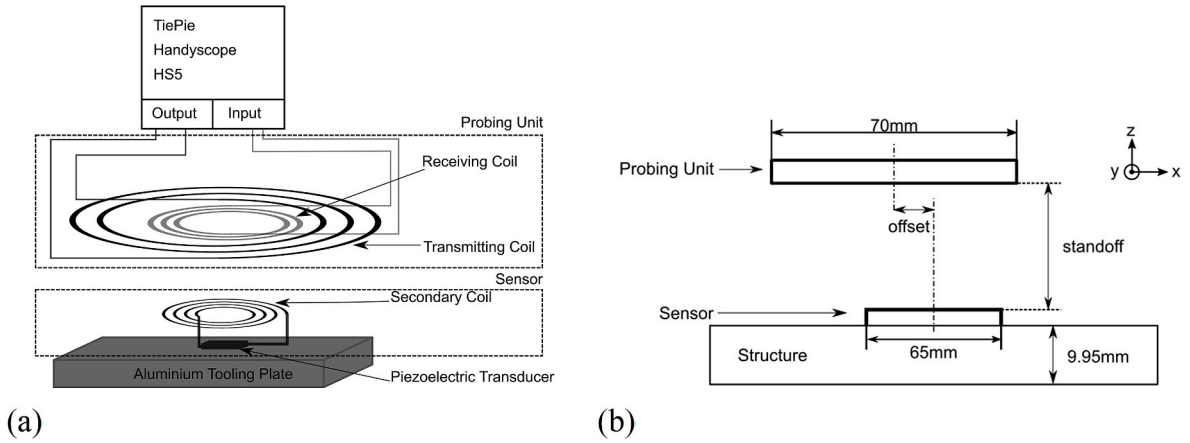

Fig. 1. Experiment setup. (a) Schematic diagram of the inductively coupled ultrasonic transducer system. (b) Schematic diagram illustrating the lateral offset and vertical standoff in the sensor system.

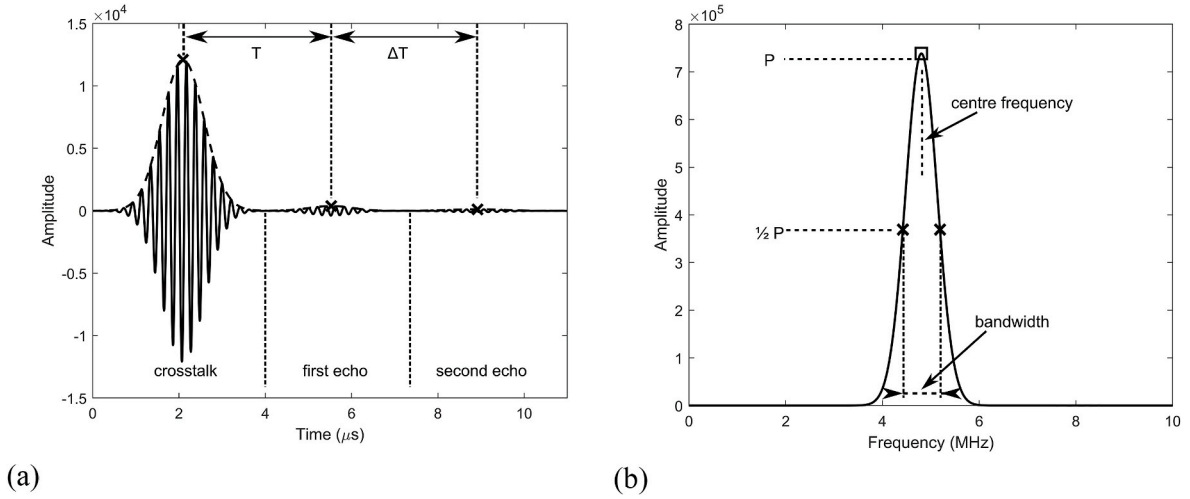

Fig. 2. Post processing techniques applied to (a) a typical time domain signal (A-scan), and (b) the frequency spectrum of the cross-talk from the time domain signal.

of the A-scan. This is because the reflected energy from the first and the second echoes can be low when the back-wall of the structure is badly corroded or when the alignment of the system is poor, whereas the cross-talk signal is guaranteed to be present. Parameters extracted from the cross-talk signals are therefore always available. The time domain cross-talk signal is extracted using a rectangular-window with a fixed length of 4 μs from the start of the signal. The peak amplitude, the full width half maximum (FWHM) bandwidth, and the centre frequency of the cross-talk are then extracted in the frequency domain as illustrated in Fig. 2 (b).

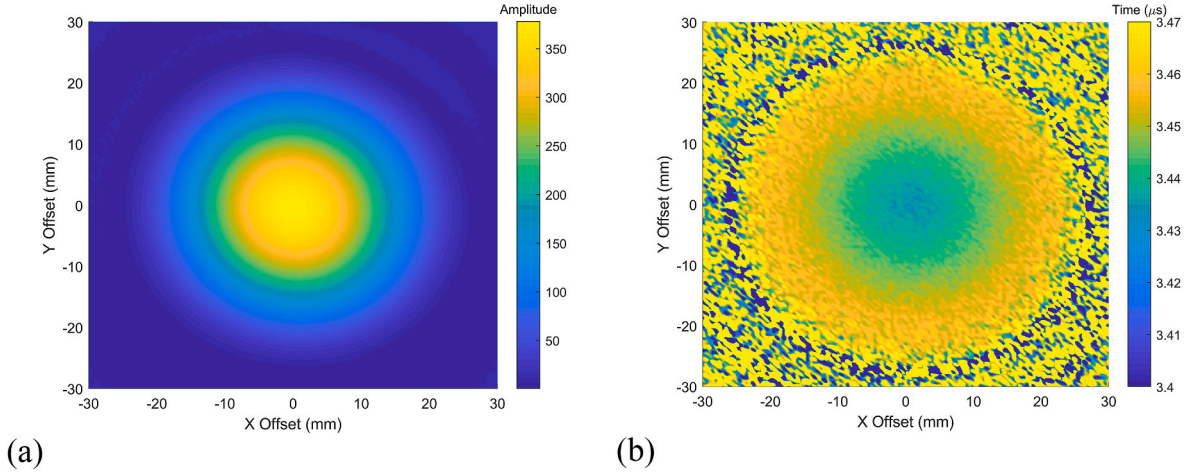

Fig. 3. Raster scan of (a) the first echo peak amplitude and (b) the first arrival time, measured in an X–Y scan with 10 mm standoff.

2.3. X–Y scan at a fixed standoff

An experiment was first conducted to investigate the effect of lateral offset of the probing unit in the X–Y plane when the standoff was fixed at 10 mm. The probing unit follows a raster scan path with a pitch of 0.5 mm, with the maximum offset of ±70 mm in the X and Y axes chosen to ensure no overlapping area between the probing unit (diameter = 70 mm) and the sensor (diameter = 65 mm) at the extremities. The temperature is controlled to ±0.5 °C while the scan takes place, to maintain the speed of sound in the plate.

The data collected in the raster scan is post processed as described in section 2.2. Fig. 3(a) shows the first echo peak amplitude for offsets of up to ±30 mm and Fig. 3(b) shows the first arrival time. It can be seen that the measured first arrival time becomes unstable, with random variations, at large offsets when the signal amplitude is low. However, at lower offsets, the measured first arrival times show systematic changes, which is the cause of the measured thickness variability that has been observed in practice. Such measured thickness variability will be addressed in section 3.

The results in Fig. 3 clearly demonstrate the axisymmetric nature of the system, with similar results obtained for the cross-talk and second echo peak amplitude. Therefore, the effect of vertical standoff can be studied by performing line scans in the X-Z plane across the centre of the sensor to reduce the amount of data collection required.

2.4. X-Z scan

In this section, both the offset and standoff are controlled in line scans in the X-Z plane (see Fig. 1), perpendicular to the installed sensor. The plane also crosses the centre of the sensor. In Fig. 3, it can be seen that the first echo peak amplitude drops as the lateral offset increases. It is important to define SNR to understand system performance in terms of relative noise. The SNR in decibels (dB) is calculated as

$$SNR = 20\log_{10}\frac{\alpha}{\sigma} \tag{1}$$

where α is the first echo peak amplitude, and σ is the random noise level taken as the root-mean-square value of the amplitudes from the last 300 samples (2.615 ms–2.621 ms) of a time domain signal, where the ultrasound will have maximally decayed and the remaining signal will be closest to random noise. Increasing lengths of window at the end of the signal for quantifying random noise level were investigated and 6 μs was found to be sufficient to provide a reliable estimate.

The scan was performed with a lateral pitch of 0.5 mm, and maximum offset of ±30 mm. The lowest standoff used in the scan is 5 mm because the sensor is normally covered with a protective coating and the probing unit cannot get any closer than this in practice. The maximum standoff is set to 15 mm to maintain a relatively high SNR over a range of offsets. A scan pitch of 1 mm in standoff is used in the data collection, but for clarity of the figures, only the results with increments of 2 mm in standoff are shown. Each measurement is post processed as described in section 2.2.

Fig. 4 shows the first echo peak amplitude in the X-Z plane. The amplitude drops as the standoff and offset increase until a minima is reached at 25 mm offset beyond which there is a small increase. The cause of the small increase in amplitude at extreme offsets is unknown, but reference to Fig. 3(b) shows that the measured arrival time at such offsets varies randomly and hence is of no use for assessing thickness. To exclude such A-scans and ensure operation in the central region where A-scans contain reliable measurable first arrival signals, the SNR at the point with 20 mm offset and 15 mm standoff, 32 dB, is set as a threshold. Measurements are accepted if the SNR is greater than 32 dB, and rejected otherwise. The valid SNR is obtained for lateral offsets within a circle of 20 mm radius and a vertical standoff between 5 mm and 15 mm.

First arrival time (T) and peak-to-peak time (ΔT) are extracted from time domain signals to provide two estimates of the remaining wall thickness, respectively,

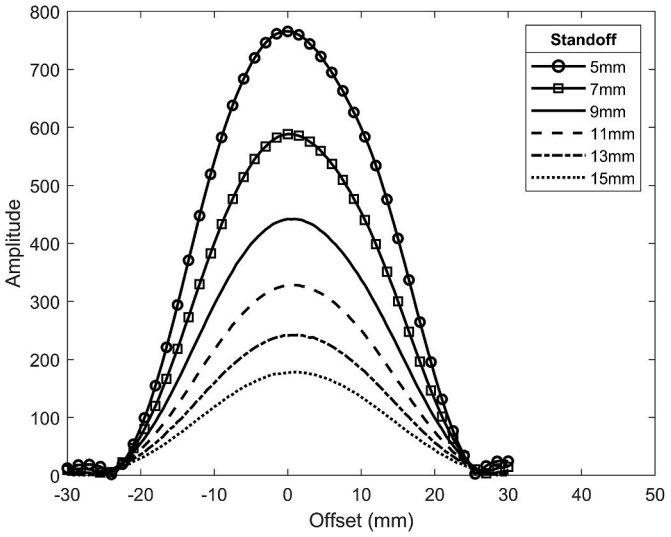

Fig. 4. Centreline scan result of the first echo peak amplitude.

$$d_T = \frac{T \cdot v}{2}$$
$$d_{\Delta T} = \frac{\Delta T \cdot v}{2}, \tag{2}$$

where v is the speed of sound in the structure.

Fig. 5 demonstrates how the measured first arrival and peak-to-peak time vary as the relative position changes, with the equivalent thicknesses calculated using eqn. (2). v is measured independently in a water immersion experiment using a single element ultrasonic probe and found to be 6386.1 m/s at 16 °C.

The thickness measurement performance within the coverage area (determined by the described acceptance threshold) is summarised in Table 1. The big range observed in peak-to-peak time at large offsets is caused by relatively low SNRs, resulting difficulty in extracting arrival times reliably. The range of the measured thickness using the first arrival time is 0.19 mm. This thickness measurement variability could be easily experienced in manual inspections using ICTS because inspectors cannot physically control the offset and standoff repeatably in every measurement. Section 3 attempts to solve the problem by developing a correction algorithm.

It is observed that peak-to-peak time varies slightly as the coil relative position changes, the separation between the peaks of the first and second back-wall echoes is not solely due to propagation of ultrasound in the plate. The piezoelectric transducer is bonded onto the plate surface and the ultrasonic path of the second back-wall echo involves a reflection off the front surface of the sample where the transducer is bonded. Consequently, the second back-wall echo signal involves an interaction with the transducer, which can be conceptually visualised as a superposition of closely-spaced reflections from both the component-transducer and the transducer-air interfaces. Both of these reflections and the separations between them will be affected by the acoustic impedance of the transducer, which will in turn is affected by its electromagnetic coupling to external circuitry.

3. Development of the correction algorithm

With the behaviour of ICTS in the presence of misalignment understood, this section develops a correction algorithm to account for these effects.

The correction algorithm is intended to work at any location with a SNR higher than 32 dB. The correction should make use of the existing

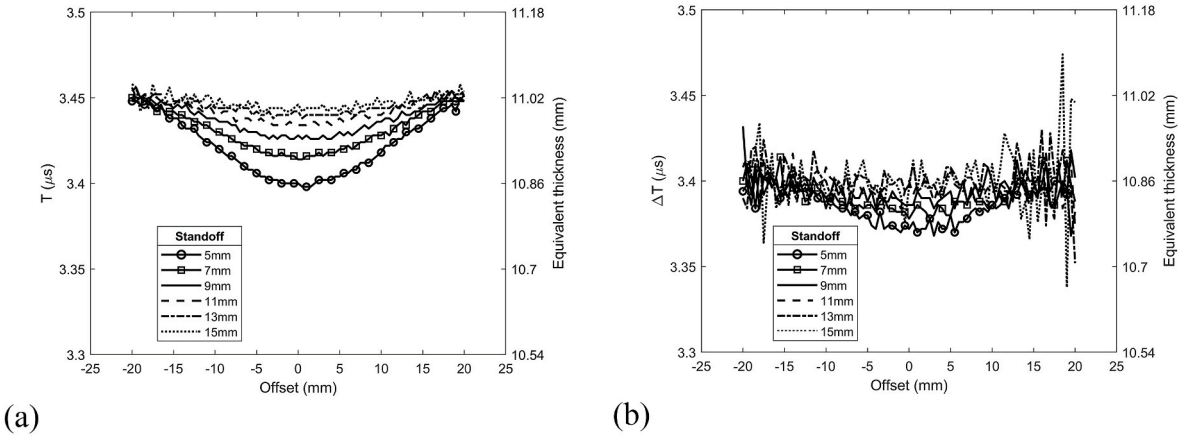

Fig. 5. X-Z scan of (a) the first arrival time and equivalent thickness, (b) the peak-to-peak time and equivalent thickness.

Table 1
Statistical comparison of the measurement performance between the estimated thicknesses using the first arrival time and the peak-to-peak time.

Thickness Estimation Metric	Mean Thickness (mm)	Mean Error (mm)	Range (mm)	Standard Deviation (mm)
T	10.97	1.02	0.19	0.04
ΔT	10.84	0.89	0.43	0.04

signal in section 2.2 (i.e., require no additional measurement) and use first arrival time instead of the peak-to-peak time to accommodate the widest possible range of back-wall conditions.

Given the independently measured speed of sound in aluminium and the measured thickness of the aluminium plate, the true time of flight through the plate is expected to be $T_{true} = 3.12$ μs. It is observed that the first arrival times shown in Fig. 5(a) are all greater than the true time of flight, suggesting that there is a system delay in ICTS and that this varies with the relative position of the probing unit and sensor. The system delay is caused by changes in the mutual inductance as the relative position of the coils alters. If this variable system delay can be eliminated more accurate thickness readings may be achieved. The system delay, τ, is defined and calculated by

$$\tau = T - T_{true}, \tag{3}$$

and is dependent on the offset and standoff.

The correction algorithm aims to determine the system delay from the cross-talk properties, on the basis that this will also be affected in some way be a change in mutual inductance between the coils in the ICTS. The cross-talk properties are predominantly governed by the mutual inductance between the transmitting and receiving coils in the probing units. Hence, the material being inspected is independent in the correction algorithm. However, the mutual inductance between the transmitting and sensor coils and between the receiving and sensor coils will also affect the cross-talk.

Unlike the first echo and second echo of the signal, the cross-talk signal is guaranteed to be present and has extremely high SNR. Fig. 6 shows how the peak amplitude, bandwidth, and centre frequency of the cross-talk change with the relative position of the coils. Of these three metrics, cross-talk bandwidth and centre frequency can both be seen to be functions of system delay. However, the objective is to determine system delay from the measurement and the graph of system delay against centre frequency is observed to have an extremely steep gradient at low values of centre frequency rending the accurate determination of system delay challenging. Hence the cross-talk bandwidth is proposed as the most useful metric for determining the system delay. Fig. 7(a) again shows the system delay plotted against the cross-talk bandwidth, and also a quadratic least squares best fit curve (in solid black line) given by an expression of the form

$$\tau_0(\Delta f) = a\Delta f^2 + b\Delta f + c, \tag{4}$$

where $\tau_0(\Delta f)$ is the estimated system delay for a measured cross-talk bandwidth Δf, and $a, b,$ and c are constants obtained from the least-squares fit. Fig. 7(b) shows the histogram of the system delay error between the fitted curve and the experimental data at each experimentally measured cross-talk bandwidth. Specifically, the maximum overestimation in the fitted system delay is 0.0096 μs, suggesting the maximum thickness underestimation by the fitted curve is 0.031 mm. The maximum underestimation in fitted system delay is 0.012 μs, equivalent to the maximum thickness overestimation of 0.038 mm. The thickness measurement precision corrected by the fitted curve is 0.069 mm, which is more than a factor of three improvement over the original thickness measurement precision of 0.19 mm in Fig. 5.

The fitted curve can be used as a correction to provide an estimate of the system delay value based on the value of cross-talk bandwidth of any measurement. The corrected system delay is then subtracted from the measured first arrival time of that measurement to yield a more accurate time of flight for thickness calculation. Applying the correction procedure, the thickness is calculated as

$$d = \frac{v}{2}[T - \tau_0(\Delta f)]. \tag{5}$$

The correction algorithm described above is applicable to new sensors at installation time, where the true thickness of the structure is either specified by the manufacturer or can be measured just before the sensor installation using other methods, such as a single element ultrasonic thickness gauge.

A slightly different philosophy can be applied to sensors that have already been installed on structures where the true thickness directly underneath the sensor is unknown and cannot be independently measured. Instead of using the correction procedure to measure the true thickness more accurately, it can be applied to more accurately measure the thickness change between measurements. In this case, the correction curve is obtained using the correlation between the first arrival time (rather than system delay) and cross-talk bandwidth measured at multiple probing unit positions, by using the quadratic least squares curve fitting:

$$\tau_1(\Delta f) = a\Delta f^2 + b\Delta f + c, \tag{6}$$

where τ_1 is the estimated first arrival time for a measured cross-talk bandwidth Δf in the calibration measurement. The underlying assumption is that for the calibration measurements

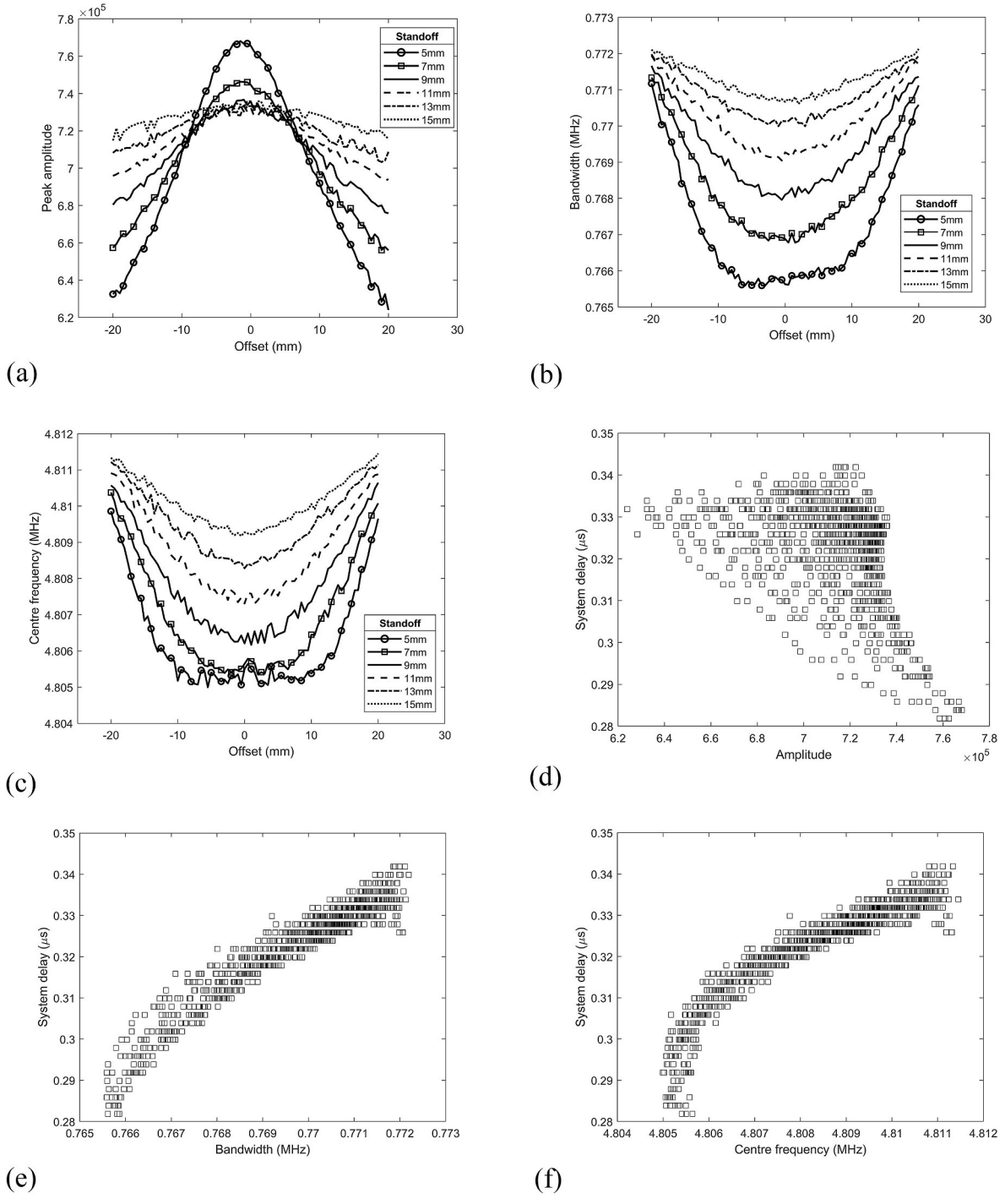

Fig. 6. X-Z scan of (a) cross-talk peak amplitude in the frequency domain, (b) cross-talk bandwidth, and (c) cross-talk centre frequency. Correlations between system delay and (d) cross-talk peak amplitude, (e) cross-talk bandwidth, and (f) cross-talk centre frequency.

$$\tau_1(\Delta f) = \tau_0(\Delta f) + \frac{2d_0}{v}, \tag{7}$$

where d_0 is the unknown initial thickness of the structure. For any subsequent measurement, the assumption is that

$$T_i(\Delta f_i) \sim \tau_0(\Delta f_i) + \frac{2d_i}{v}, \tag{8}$$

where d_i is the current thickness and Δf_i is the cross-talk bandwidth of the current measurement. Hence the measure of thickness change from the calibration measurement is calculated as

$$T_i(\Delta f_i) - \tau_1(\Delta f_i) = \left[\tau_0(\Delta f_i) + \frac{2d_i}{v}\right] - \left[\tau_0(\Delta f_i) + \frac{2d_o}{v}\right] = \frac{2}{v}(d_i - d_0). \tag{9}$$

Furthermore, a measure of thickness difference between two later first arrival time measurements, T_i and T_j, with associated cross-talk bandwidths, Δf_i and Δf_j, can also be calculated from

$$\begin{aligned}[T_i(\Delta f_i) - \tau_1(\Delta f_i)] - [T_j(\Delta f_j) - \tau_1(\Delta f_j)] &= \frac{2}{v}(d_i - d_0) - \frac{2}{v}(d_j - d_0) \\ &= \frac{2}{v}(d_i - d_j).\end{aligned} \tag{10}$$

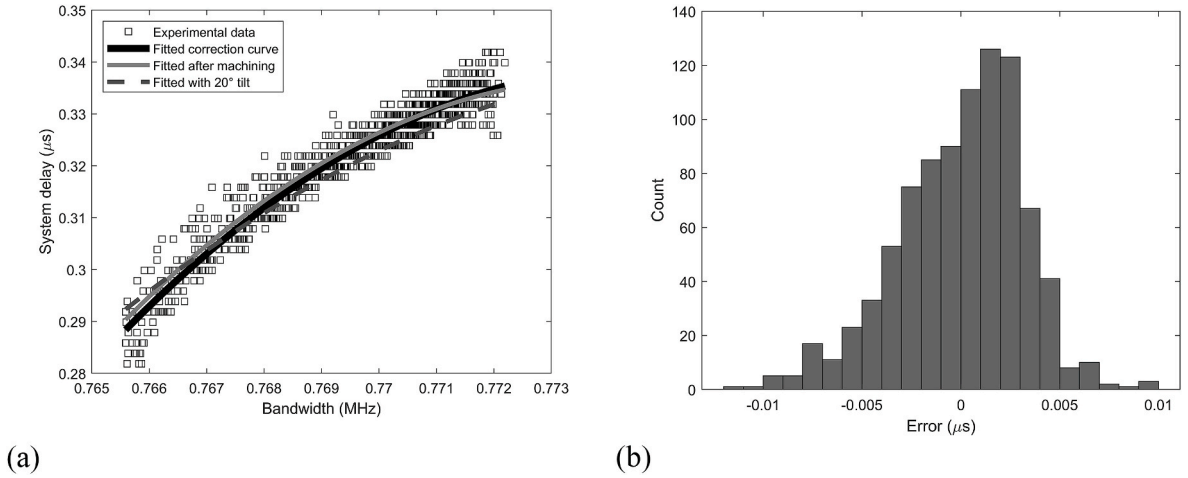

Fig. 7. (a) The fitted correction curve for the correction algorithm, (b) histogram of the time error between the experimental data and the fitted correction curve.

Although the newly measured first arrival time offers an insight into the absolute remaining wall thickness, the correction algorithm yields a more accurate thickness change between two measurements, which provides critical information on the rate of localised structural degradation.

The correction algorithm was also tested on a steel plate which is more commonly used in real applications, the results show that the correction algorithm is equally valid as the cross-talk properties are predominantly governed by the mutual inductance between the coils in the ICTS system.

Rotational misalignment of the ICTS was also investigated as inspectors may also tilt the probing unit while experiencing translational misalignment. An X-Z scan was conducted with the probing unit tilted 20° from the horizontal, the correction curve generated is shown in Fig. 7(a) in dashed line, which is comparable to the correction curve generated without any tilt. The fact that a large tilt of 20° hardly alters the correction curve suggests that translational and rotational misalignment have similar effects on measurement accuracy and that both can be corrected using a common correction curve.

4. Demonstration of measurement performance improvement using the correction algorithm

To demonstrate the measurement performance improvement provided by the correction algorithm, further experiments and comparisons are described in this section.

4.1. Direct comparison

With the X-Z scan data collected in section 2.4, the measured thickness using the uncorrected first arrival time is compared with the corrected thickness using the correction algorithm, and the results are plotted in Fig. 8. Note that the true thickness of the sample is 9.95 mm as indicated by the dashed line.

The histogram in Fig. 8 and the statistical parameters shown in Table 2 indicate that the correction algorithm has greatly improved the measurement performance of the ICTS system within the coverage area. The mean of the corrected thickness is identical to the true thickness of the aluminium plate, the range and the standard deviation are reduced significantly. Therefore, applying the correction algorithm improves both the measurement accuracy and precision. It can also be seen from Fig. 8 that the corrected thickness is more normally distributed than the uncorrected thickness distribution, which means that the performance of the correction algorithm can be more easily characterised.

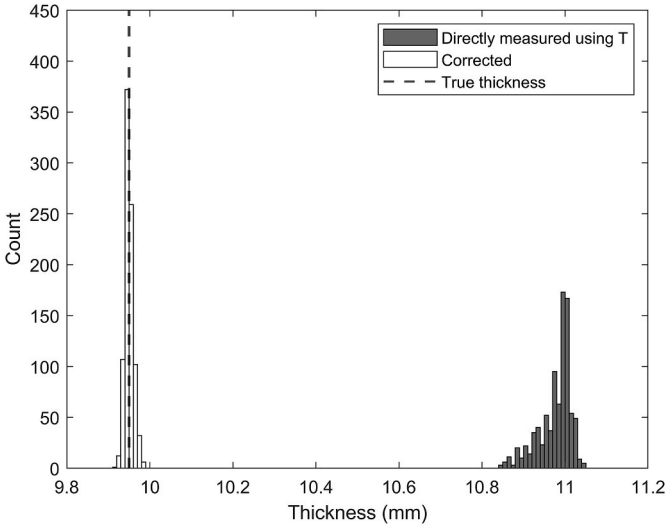

Fig. 8. Comparison between the directly measured thickness using the first arrival time and the corrected thickness in the X-Z scan.

Table 2
Statistical comparison of the measurement performance between the directly measured thickness using the first arrival time and the corrected thickness using the correction algorithm.

Method	Mean Thickness (mm)	Mean Error (mm)	Range (mm)	Standard Deviation (mm)
Directly measured	10.98	1.03	0.19	0.04
Corrected	9.95	0.00	0.07	0.01

4.2. Thickness variability in repeat measurements

From a SHM point of view, the thickness change between two measurements must be measured accurately. Before the correction algorithm was developed, accurate thickness change could only be measured if the alignment between the probing unit and the sensor was almost perfectly repeated between two measurements, challenging for manual placement of the probing unit. With the correction algorithm deployed, accurate measurement of thickness change is possible even without perfect alignment.

Three repeat X-Z scans were conducted within the coverage area to explore the maximum thickness repeatability error at every probing unit

location without applying the correction algorithm and to compare it with the maximum variability of the corrected thickness.

The maximum thickness difference at each probing unit location over three measurements without correction is shown in Fig. 9(a), and the cumulative distribution function plot of the thickness repeatability error is demonstrated in Fig. 9(b). In the coverage area, the maximum thickness repeatability error detected at a certain location is 0.064 mm and the standard deviation is 0.0084 mm. These represent the repeatability limits that can be achieved without correction if the probing unit is positioned at the accuracy of our commercial scanning system (nominally ±0.05 mm per 300 mm movement). By contrast, as shown in Table 2, the range and the standard deviation of the corrected thickness in the coverage area are 0.07 mm and 0.01 mm, respectively. This shows that the correction algorithm has enabled comparable measurement performance to be achieved with probing unit lateral and vertical misalignments of up to 20 mm and 10 mm.

4.3. Detection of thickness loss in the structure

The aluminium plate is machined to check if the correction algorithm is capable of detecting a small thickness loss. The thickness was reduced from 9.95 mm to 9.86 mm, with the thickness loss introduced being approximately 1% of the original thickness. An X-Z scan was carried out on the machined sample and a new correction curve calculated, which is also shown in Fig. 7. The similarity of the correction curves before and after machining demonstrate that the calibration process is repeatable. For subsequent analysis only the original correction curve is used as this would be the situation in practice.

Fig. 10(a) shows the histograms of the uncorrected thickness measured before and after machining. Clearly there is a region where the measured thickness readings overlap between these two sets of data, resulting that the thickness loss could be zero or negative values while the true thickness loss being 0.09 mm. By applying the correction algorithm, as shown in Fig. 10(b), the corrected thickness readings from those two datasets are clearly separated from each other with no overlap, leading to 100% success rate of detecting a positive thickness loss. Both histograms in Fig. 10(b) are fitted with a normal distribution function to make statistical comparisons. The fitted normal distributions have the same mean and standard deviation as the sample mean and standard deviation, listed in Table 3. The difference between the mean of the corrected thickness before and after the thickness loss exactly matches with the true thickness loss to within 0.01 mm. According to the fitted normal distribution probability density functions for the corrected thickness, the probability of measuring a thickness greater than 9.95 mm after machining and the probability of measuring a thickness smaller than 9.86 mm before machining are 3.19×10^{-14} and 1.13×10^{-19}, respectively, by looking up the Z score table. This serves to demonstrate the merits of the compensation approach.

To further demonstrate the effect of misalignment between measurements and the performance of the correction algorithm, the uncorrected and corrected thickness losses calculated with all possible combinations of probing positions before and after machining are shown in Fig. 11(a) and (b), respectively. In the presence of misalignment between two measurements, the measured thickness after machining could exceed the measured thickness before machining, resulting in a negative thickness loss as shown in Fig. 11(a), in the case without correction. By contrast, the corrected thickness loss is always positive, confirming that a thickness loss is guaranteed to be detected.

Although the uncorrected and corrected thickness loss have the same mean of 0.09 mm, the uncorrected thickness loss has a range of 0.40 mm and a standard deviation of 0.056 mm, whereas the corrected thickness loss has a narrower range of 0.15 mm and a smaller standard deviation of 0.016 mm. Therefore, the correction algorithm has greatly improved the measurement performance in the case of thickness loss, even with inconsistent probing positions between measurements.

5. Quick fit method for correction curve generation

The key element of the correction algorithm is the correction curve, which needs to be fitted to experimental data acquired during the calibration phase. Fewer experimental data points for curve fitting are desired for ease of implementation in practice as opposed to 891 data points used in Fig. 7(a). The experimental data required for curve fitting consists of first arrival times and cross-talk bandwidth of a signal. This requires measurements to be taken at a range of standoffs and offsets to cover the full range of cross-talk bandwidth, so that the correction algorithm can work within the whole coverage area accurately.

To fit the correction curve to the experimental data efficiently and accurately, the cross-talk bandwidth range can be split into a number of bins with the number of input points for each bin ideally identical to reduce weighting bias in the curve fitting process. The cross-talk bandwidth changes as the relative position changes, so that cross-talk bandwidth measurements can fall into different bins. The bin width automatically adapts as new measurements are acquired while the number of bins is fixed.

The exact standoff and offset cannot be easily controlled during manual data collection in the field. Therefore, the most efficient and easiest way to generate the correction curve is to randomly move the probing unit relative to the sensor while the calibration measurements are made, in order to create offset and standoff variations while

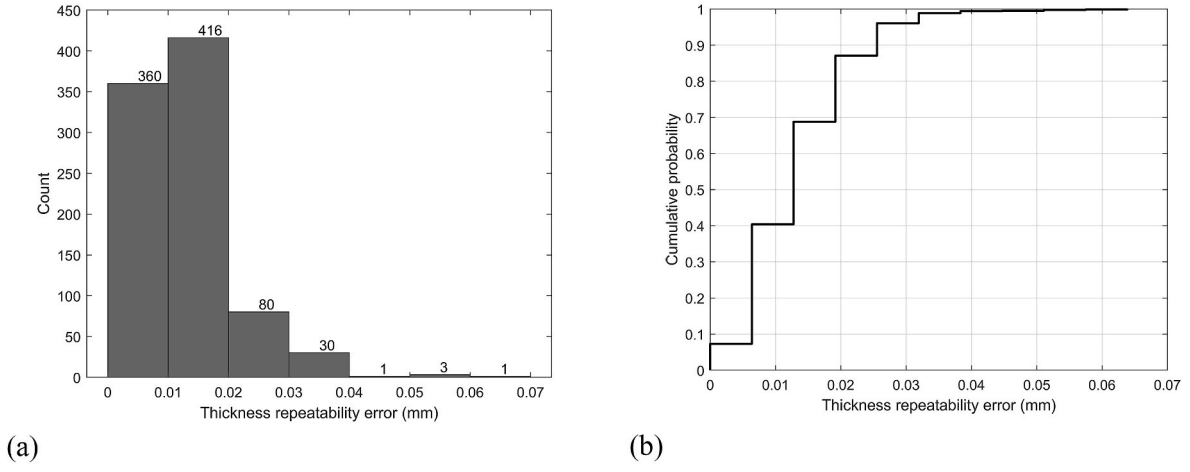

Fig. 9. (a) Histogram of the maximum thickness difference at each location in the X-Z scan over three repeat measurements, and (b) cumulative distribution function plot of the thickness repeatability error.

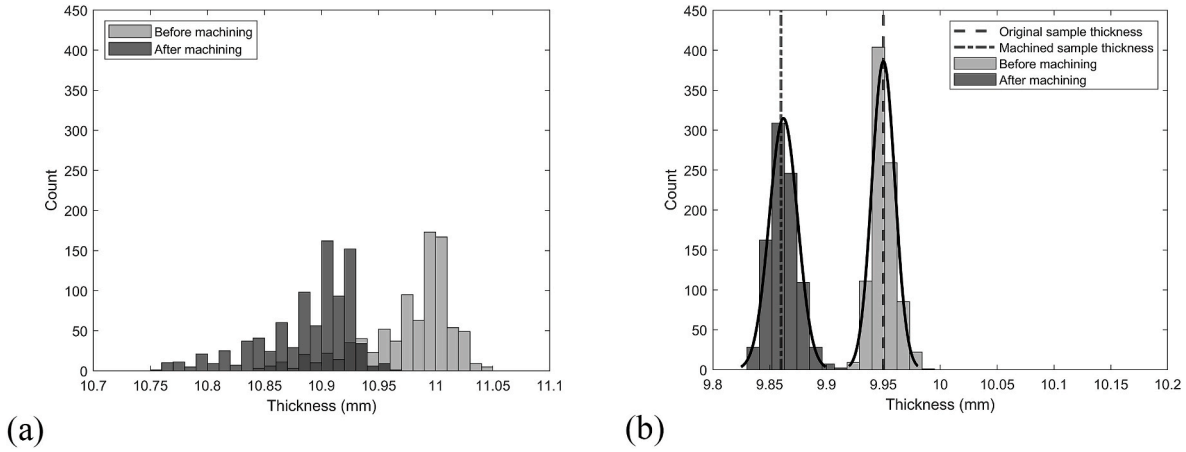

Fig. 10. Histograms of (a) the directly measured thickness using the first arrival time before and after machining, (b) the corrected thickness before and after machining, with a normal distribution fit.

Table 3
Sample mean and standard deviation of the corrected thickness before and after thickness loss.

Sample Name	Sample Mean (mm)	Sample Standard Deviation (mm)
Before machining	9.95	0.010
After machining	9.86	0.012

measurements are acquired continuously. SNR is used in this process to accept or reject measurements. As each new measurement is acquired and the number of points in each bin is equal, the curve fitting is repeated based on the available data. The data collection is finished either when the changes in the fitted curve are less than a prescribed amount or when the number of points in each bin reaches a limit.

The optimal number of bins is investigated by checking how fast the residual sum of squares between the experimental data and the fitted curve converges as the number of points in each bin increases. Results show that as the number of bins increases, the residual sum of squares converges with fewer input points. However, manual data collection is more challenging for inspectors with more bandwidth bins because the range of standoffs and offsets combinations that must be covered is higher. On the other hand, fewer bandwidth bins may need more input points in each bin to accurately fit a correction curve, but inspectors are expected to find this easier due to the less restricted movement of the probing unit. Three equal-sized, contiguous bandwidth bins are selected for the quick fit method as a compromise between the ease of manual data collection and number of input points. Fig. 12(a) shows the convergence plot between the residual sum of squares against the number of input points in each bin, the input points are randomly selected from the same set of experimental data used in previous sections. 100 realisations are implemented for each number of input points, the maximum and minimum residual sum of squares of 100 realisations are demonstrated. The residual sum of squares quickly converges after 20 points from each bin, leading to a total 60 input points for generating a correction curve reliably. Fig. 12(b) demonstrates 10 realisations of the correction curve fitted using the quick fit method with 20 points from each bin, which agrees well with the complete correction curve computed from all 891 measurements. For example, if the worst fit of the 10 realisations is used to correct measured thickness before machining, it achieves a comparable measurement performance (i.e., almost identical mean, mean error, range, and standard deviation to the data shown in Table 2.) to the complete correction curve.

6. Conclusion

The current paper has investigated the effect of coil misalignment of an ICTS on the received signal. Translational and rotational misalignment leads to variability in the thickness calculated from the measurement. Industrial sites may have a huge number of thickness

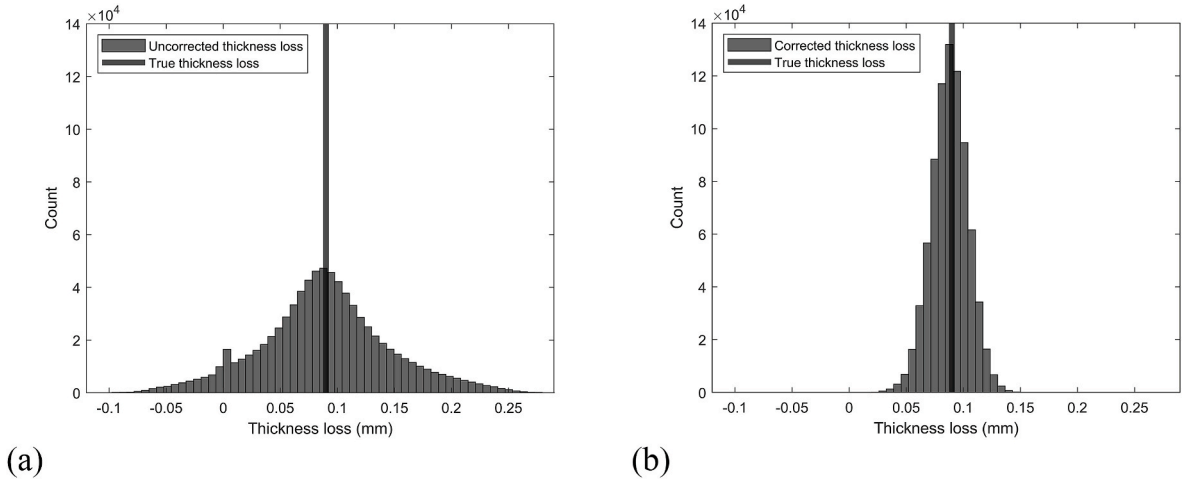

Fig. 11. Histogram of the (a) uncorrected and (b) corrected thickness loss before and after machining in the X-Z scan, with all combinations of probing positions between these two scans considered.

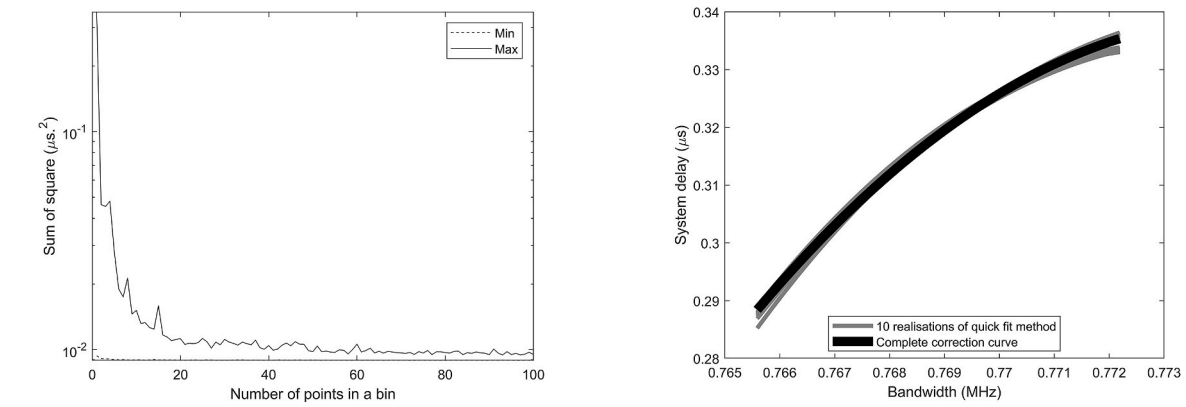

Fig. 12. (a) Convergence plot of residual sum of squares of the fitted correction curve against number of points in a bin for quick correction curve generation. (b) Comparison between the complete correction curve computed from 891 measurements and 10 example correction curves fitted using the quick fit method with 20 input points in each of 3 bins.

measurement locations (TMLs), and if inspections are carried out manually then operators will be unable to ensure perfect alignment at all locations leading to an artificially large spread on indicated thicknesses being recorded [6,14]. A correction algorithm has been developed to account for the effect of misalignment on thickness measurements, providing flexibility of probe alignment with up to 20 mm lateral offset and 10 mm vertical standoff for ease of inspection in the field. The correction algorithm greatly improves the system measurement performance by enabling smaller thickness changes to be measured with higher accuracy and precision. On a 9.95 mm thick flat and smooth aluminium plate, it is able to reduce the thickness measurement precision from 0.19 mm to 0.07 mm in the coverage area. It can also unambiguously detect a small thickness loss of 0.09 mm thickness loss; without correction, ICTS could fail to detect any loss.

The use of the correction algorithm developed for ICTS can lower the positioning requirement for robots while navigating between installed sensors due to the 20 mm maximum offset allowance, which makes robotic inspections of ICTS potentially viable to save cost and time of inspections.

Further investigations will firstly investigate how temperature affects the implementation of the proposed correction algorithm, temperature variation in the fields effectively changes the speed of sound in the structure, leading to changes in thickness calculation. Besides, the mechanical properties of the adhesive layer are also affected by temperature. Future work of testing the correction algorithm on curved structures (e.g. pipes, elbows) is also required, to further enhance the measurement performance and practicality of the ICTS.

CRediT authorship contribution statement

Yangjie Chen: Conceptualization, Methodology, Software, Validation, Formal analysis, Investigation, Data curation, Writing – original draft, Writing – review & editing, Visualization, Project administration. **Jie Zhang:** Conceptualization, Methodology, Formal analysis, Data curation, Writing – review & editing, Supervision. **Anthony J. Croxford:** Conceptualization, Methodology, Formal analysis, Resources, Data curation, Writing – review & editing, Supervision, Funding acquisition. **Paul D. Wilcox:** Conceptualization, Methodology, Formal analysis, Data curation, Writing – review & editing, Supervision, Funding acquisition.

Declaration of competing interest

The authors declare that they have no known competing financial interests or personal relationships that could have appeared to influence the work reported in this paper.

Acknowledgements

This work is supported by EPSRC Centre for Doctoral Training in Future Innovation in Non-Destructive evaluation (FIND) [grant number EP/S023275].

References

[1] Holmes C, Drinkwater BW, Wilcox PD. Post-processing of the full matrix of ultrasonic transmit-receive array data for non-destructive evaluation. NDT E Int 2005;38:701–11.
[2] Drinkwater BW, Wilcox PD. Ultrasonic arrays for non-destructive evaluation: a review. NDT E Int 2006;39:525–41.
[3] Zhang J, Drinkwater BW, Wilcox PD, Hunter AJ. Defect detection using ultrasonic arrays: the multi-mode total focusing method. NDT E Int 2010;43:123–33.
[4] Fromme P, Wilcox PD, Lowe MJS, Cawley P. On the development and testing of a guided ultrasonic wave array for structural integrity monitoring. IEEE Trans Ultrason Ferroelectrics Freq Control 2006;53:777–85.
[5] Croxford AJ, Wilcox PD, Drinkwater BW, Konstantinidis G. Strategies for guided-wave structural health monitoring. Proceedings of the Royal Society A 2007;463:2961–81.
[6] Cegla F. Manual UT vs permanently installed sensors", 7th European workshop on structural health monitoring. 2014. p. 631–8.
[7] Farrar CR, Worden K. An introduction to structural health monitoring. Proceedings of the Royal Society A 2006;365:303–15.
[8] Zhong A J Croxford, Wilcox PD. Investigation of inductively coupled ultrasonic transducer system for NDE. IEEE Trans Ultrason Ferroelectrics Freq Control 2013;60:1115–25.
[9] Bogue R. The role of robotics in Non-destructive Testing. Ind Robot 2010;37:421–6.
[10] Dobie G, Summan R, MacLeod C, Pierce G, Galbraith W. An automated miniature robotic vehicle inspection system. AIP Conf Proc 2014;1581:1881–8.
[11] Yuan J, Wu X, Kang Y, Huang C. Development of an inspection robot for long-distance transmission pipeline on-site overhaul. Ind Robot 2009;36:546–50.
[12] Jarvis R, Farinha A, Kovac M, Cegla F. NDE sensor delivery using unmanned aerial vehicles. Insights 2018;60:463–7.
[13] Miro JV, Ulapane N, Shi L, Hunt D, Behrens M. Robotic pipeline wall thickness evaluation for dense nondestructive testing inspection. J Field Robot 2018;35:1293–310.
[14] McGregor A, Dobie G, Pearson NR, Macleod CN, Gachagan A. Determining position and orientation of a 3-wheel robot on a pipe using an accelerometer. IEEE Sensor J 2020;20:5061–71.
[15] Liu H, Pang G. Accelerometer for mobile robot positioning. IEEE Trans Ind Appl 2001;37:812–9.
[16] Michaels JE, Lee S, Croxford AJ, Wilcox PD. Chirp excitation of ultrasonic guided waves. Ultrasonics 2013;53:265–70.
[17] Cooper M. Wireless battery-free ultrasonic thickness measurement patches for CO_2 absorber. Inspectioneering J 2021;27:1–7.